

Interface state-based bound states in continuum and below-continuum-resonance modes with high-*Q* factors in the rotational periodic system

Jialing Yang(杨嘉玲), Aoqian Shi(史奥芊), Yuchen Peng(彭宇宸), Peng Peng(彭鹏), and Jianjun Liu(刘建军)
Citation: Chin. Phys. B, 2024, 33 (**8**): 084206. DOI: 10.1088/1674-1056/ad4630

What follows is a list of articles you may be interested in

Topological edge and corner states of valley photonic crystals with zipper-like boundary conditions

Yun-Feng Shen(沈云峰), Xiao-Fang Xu(许孝芳), Ming Sun(孙铭), Wen-Ji Zhou(周文佶), and Ya-Jing Chang(常雅箐)
Chin. Phys. B, 2024, 33 (**4**): 044203. DOI: 10.1088/1674-1056/ad1e6a

Enhancing the Goos-Hänchen shift based on quasi-bound states in the continuum through material asymmetric dielectric compound gratings

Xiaowei Jiang(江孝伟), Bin Fang(方彬), and Chunlian Zhan(占春连)
Chin. Phys. B, 2024, 33 (**3**): 034206. DOI: 10.1088/1674-1056/acf661

Evolution of polarization singularities accompanied by avoided crossing in plasmonic system

Yi-Xiao Peng(彭一啸), Qian-Ju Song(宋前举), Peng Hu(胡鹏), Da-Jian Cui(崔大健), Hong Xiang(向红), and De-Zhuan Han(韩德专)
Chin. Phys. B, 2023, 32 (**1**): 014201. DOI: 10.1088/1674-1056/ac728d

Bound states in the continuum in metal—dielectric photonic crystal with a birefringent defect

Hongzhen Tang(唐宏珍), Peng Hu(胡鹏), Da-Jian Cui(崔大健), Hong Xiang(向红), and Dezhuan Han(韩德专)
Chin. Phys. B, 2022, 31 (**10**): 104209. DOI: 10.1088/1674-1056/ac6db6

Bound states in the continuum on perfect conducting reflection gratings

Jianfeng Huang(黄剑峰), Qianju Song(宋前举), Peng Hu(胡鹏), Hong Xiang(向红), and Dezhuan Han(韩德专)
Chin. Phys. B, 2021, 30 (**8**): 084211. DOI: 10.1088/1674-1056/abeee4

Interface state-based bound states in continuum and below-continuum-resonance modes with high-Q factors in the rotational periodic system

Jialing Yang(杨嘉玲)[1], Aoqian Shi(史奥芊)[1], Yuchen Peng(彭宇宸)[1], Peng Peng(彭鹏)[1], and Jianjun Liu(刘建军)[1,2,†]

[1] *Key Laboratory for Micro/Nano Optoelectronic Devices of Ministry of Education, School of Physics and Electronics, Hunan University, Changsha* 410082, *China*

[2] *Greater Bay Area Institute for Innovation, Hunan University, Guangzhou* 511300, *China*

(Received 25 February 2024; revised manuscript received 24 April 2024; accepted manuscript online 2 May 2024)

We have introduced a new approach to calculate the orbital angular momentum (OAM) of bound states in continuum (BICs) and below-continuum-resonance (BCR) modes in the rotational periodic system nested inside and outside by transforming the Bloch wave number from the translational periodic system. We extensively classify and study these BICs and BCR modes, which exhibit high-quality (high-Q) factors, in different regions relative to the interface of the system. These BICs and BCR modes with a high-Q factor have been studied in detail based on distinctive structural parameters and scattering theory. The outcomes of this research break the periodic limitation of interface state-based BICs, and realize more and higher symmetry interface state-based BICs and BCR modes. Moreover, we can control the region where light is captured by adjusting the frequency, and show that the Q factor of BICs is more closely related to the ordinal number of rings and the rotational symmetry number of the system.

Keywords: bound states in the continuum, below continuum resonance modes, high-quality factors

PACS: 42.70.Qs, 42.60.Da, 78.67.Pt **DOI:** 10.1088/1674-1056/ad4630

1. Introduction

BICs with infinite lifetimes, which exist in the frequency domain with matched energy and momentum,[1–3] are also known as embedded eigenstates in the continuum. One of the most intensively studied BICs is the symmetry-protected BIC, which can easily be found in photonic crystal (PhC) with a certain symmetry.[4–7] The construction of topological optical systems in PhC represents a fundamental approach towards achieving optical signal tight binding or low local loss.[8–10] PhC is widely used as the material to realize BIC due to its unique restrictions and transmission characteristics.[11–13] BICs can be viewed as special resonances with infinite Q factors because different radiation channels interfere destructively with each other in the far-field,[11,14,15] which makes them highly desirable for applications such as PhC lasers,[16] sensors,[17–19] beam shift,[20–23] filters,[24,25] fibers based on BIC,[26] and optical switches[27] that require high-Q factors. Furthermore, BICs hold great potential for further research and development.[28–30]

Quasi-BICs in the region of the photonic band gap (PBG) have been realized with extremely high-Q factors (i.e., near-BICs) in circular PhC.[5,31–33] However, these previous works were limited to simple circular systems and focused primarily on the relationship between the Q factors of symmetry-protected near-BICs and the number of scatterers. It is important to note that the Q factors of BCR modes in these systems were found to be lower than those of near-BICs. To enhance the practical utility of BCR modes within circular structures, it is essential to design a rotational symmetry structure with multimode scattering. Those designs can significantly reduce large bending losses and improve the Q factor.[26,32,33] To establish a deeper connection between the Q factor and the structure of the rotational periodic system, it is necessary to introduce an analysis of rotational symmetry. Furthermore, in order to expand the frequency range of the trapped light in the region of PBG in a new generation of optical fibers of a circular system,[33] we refer to the BICs from translational periodic systems[34–38] to introduce more BIC (BCR modes) in the region of bulk bands. Moreover, it is necessary to design off-Γ BICs in order to improve the fabrication tolerance of the device. In practice, only the symmetry-protected BICs at the Γ point are vulnerable to damage. Distinct from interface state-based BICs and Brillouin zone folding-induced BICs in a translational periodic system,[37,38] the introduction of rotational symmetry within PhC can generate a greater number of symmetry-protected BICs.[39,40]

2. Models and theory

In this paper, we have successfully achieved all BICs and BCR modes based on the bulk bands of two PhCs in the rotational periodic system. This achievement is expected to offer more potential applications for PhC devices of a circular array.

†Corresponding author. E-mail: jianjun.liu@hnu.edu.cn

© 2024 Chinese Physical Society and IOP Publishing Ltd

We have established the interface state-based BICs (at and off-point) and BCR modes (off-Γ point) with C_{6v} (C_{3v}) symmetry. These off-Γ BICs (BCR modes) in the rotational periodic system address the challenges of high loss attributed to interface scattering and high cross-section material loss in actual manufacturing. Our efforts extended the scattering theory of the rotational periodic system from C_{6v} symmetry to C_{nv} symmetry, varying the parameters accordingly. The results demonstrate that the Q factor of symmetry-protected BICs increases with MN.

We designed a rotational periodic system consisting of two rotational symmetry PhCs nested inside and outside, as shown in Fig. 1.

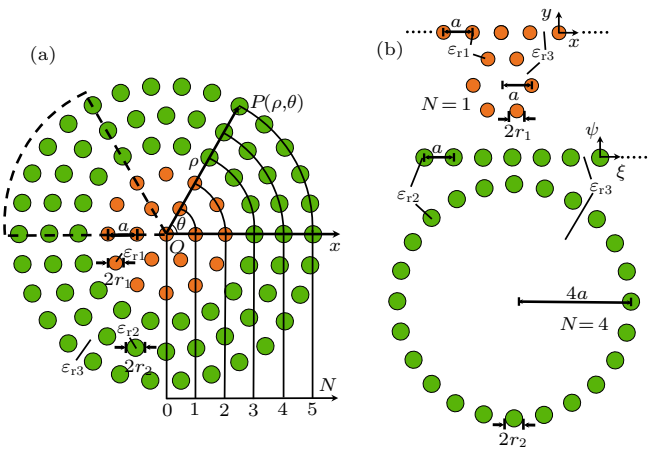


Fig. 1. (a) The rotational periodic system consisting of two rotational symmetry PhCs with C_{6v} symmetry (inside PhC1, outside PhC2). The relative permittivity and radius of the orange and green circular scatterers are $\varepsilon_{r1} = 9$, $r_1 = 0.24a$, and $\varepsilon_{r2} = 15$, $r_2 = 0.28a$.[37] Inside the fan-shaped dotted line is the minimum rotation unit of the rotational periodic system. (b) The circular PhC of the rotational periodic system, above the circular PhC, is its corresponding infinite periodic PhC chain.

As shown in Fig. 1(a), the system is designed with the central scatterer as the center of rotation. We defined a as the lattice constant of this system. It is known that in some PhCs possessing a Dirac-like cone at $k = 0$ derived from monopole and dipoles excitation, a small perturbation is sufficient to create interface states.[41] We chose a material with two different relative permittivities which will cause this interface state as the scatterer P in this paper. The polar coordinates of any scatterer P (the scatterer inside PhC1, outside PhC2) in space can be determined using this center of rotation

$$P(\rho,\theta) = P(aN, 2\pi n/(MN)). \tag{1}$$

The parameters for the model are defined as follows: a, N, and M represent the lattice constant, the ordinal number of the concentric ring, and the rotational symmetry number in the model, respectively, with its specific factor determined by the number of scatterers in the first ring outward from the center (in the model depicted in Fig. 1, $M = 6$). Additionally, n represents the ordinal number of the n-th scatterer on the N-th ring, with its factor taken in the counterclockwise direction. It is important to note that n equals 1 on the polar axis. The circular PhC is constructed by periodically rolling infinite periodic PhC chains in Fig. 1(b), with an angular period of $2\pi/(MN)$. The linear Bloch wave number $k_n = 2\pi n/a$ ($n = 0, \pm1, \pm2, \ldots MN$), a corresponds to a period length of the infinite periodic array.[6,33] Consequently, this transformation yields the azimuth Bloch wave number $k_m = 2\pi m/(MN)$ for the azimuth Bloch wave number of the circle array. The rotational period system can be viewed as consisting of circular PhCs with a combination of circular ordinal numbers from 0 to 5. Such a system similarly has symmetry-protected BICs in circular PhCs, which can certainly be explained through symmetry analysis.[14] Therefore, we can also calculate the k_m of these symmetry-protected BICs by the above transformation in the rotational periodic system. Similarly, in order to calculate the k_m of BIC (BCR modes) inside and in the interface of a rotational periodic system, translational periodic systems with an interface should be designed. In this paper, we investigate structures similar to those studied in Ref. [37] to connect the rotational periodic system of C_{6v} symmetry to the interface state-based BICs and define the k_m as $k_{||}$ in the rotational periodic system.

Based on the scattering theory of an infinitely long periodic array, specifically the dielectric column linear array,[6,14,18,33] it has been observed that the incident and emanating wave are linked to m (OAM). The Mie scattering theory[42] of magnetic resonance has been introduced to describe a multi-particle system. This theory is combined with multiple scattering theory to convert the scattering field in the rotational periodic system into a series of functions that are related to both the incidence and scattering amplitudes. As a result, the electromagnetic resonance problem can be transformed into an eigenvector problem of scattering amplitudes without considering the incidence field.

Following Ref. [43] and seeing quite a similar procedure for the Neumann boundary conditions at the surfaces of rigid cylinders,[44] we present the general E-polarized solution at the vicinity of the g-th scatterer for the electric field directed along the scatterers. We set g as the g-th scatterer on the N_g-th ring (g, $g+1$, $g+2\ldots$), with its factors taken in the counterclockwise direction. For the incident wave on the $(g+1)$-th scatterer,

$$E_{\text{inc}} = H_n^{(1)}(k_0 r_{g+1})\, \mathrm{e}^{\mathrm{i}n\phi}, \tag{2}$$

where the first term presents the incident wave from a point-like source placed at the center of circular array $x = 0$, $y = 0$. E_{inc} represents the incident wave from a point source assumed to be located at the geometric center, ϕ is the polar coordinates of the radius vector r_{g+1} in the coordinate systems of the near-field zone.

The far-field zone concerning particular model parameters, outside the scatterers for $r_g > a$, the solution with the Bloch wave number k_n takes the following form:

$$E_{z,n} = \sum_m \sum_{g=1} a_{mn}^{-}(1)\exp[\mathrm{i}k_n(g-1) + \mathrm{i}m(\phi-\varphi_g)]H_m^{(1)}(k_0 r_g)\,\mathrm{e}^{\mathrm{i}m\phi}. \quad (3)$$

3. Results and discussion

Due to the lack of translational symmetry, the band structure of the rotational periodic system cannot be analyzed based on the Brillouin zone. We propose a novel approach to understanding the bound states in the rotational periodic system. Specifically, we designed the translational periodic system, which can represent the frequency position of BICs and BCR modes (see Sections A and B of the supplementary material). This information is illustrated in Fig. 2.

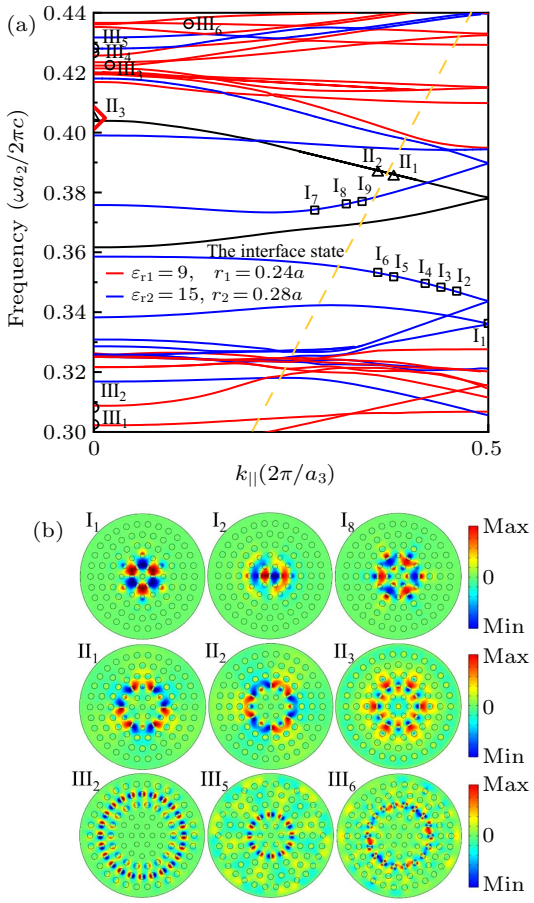


Fig. 2. (a) Projected band structure of the long-strip supercell and BICs (BCR modes) of the rotational periodic system. BICs (BCR modes) on the blue, black and red curves are marked with squares, triangles and circles. The black curve indicates the folded interface state and resonances extending into the bulk band. The yellow dotted line represents the light line of air, the black line represents the interface state. (b) E_z field distributions of BICs and BCR modes in the rotational system are shown, with each row corresponding to a type of BIC (BCR mode).

The bound states in the calculated rotational periodic system are classified according to the light line in Fig. 2(a). The field distribution is obtained by full-wave simulation. Figure 2(b) shows the E_z field distributions of the bound states labeled in Fig. 2(a). The E_z field (I_1, I_2, I_8) in Fig. 2(b) shows that the electromagnetic distributions meet C_{3v} and C_{2v} symmetries, and their positions on the projected bands of the long-strip supercell are at non-0 point (non-C_{6v} symmetry-protected BICs (BCR modes)), conforming to the general distribution of their positions on the projected bands.

It can be found that the position of the BICs (BCR modes) of the rotational periodic system in the projected bands of the square lattice PhC in Fig. 2(a) corresponds one-to-one with the position (external representation) of the local electromagnetic area in different PhCs in Fig. 2(b). By combining two positions, the BICs (BCR modes) in this frequency band are classified. Type I BCR modes (I_1–I_6) and type I BICs (I_7–I_9) exist in the PBG of PhC2 but in the bulk band of PhC1 (blue curve) and PhC1 in the rotational periodic system. The type II BCR mode (II_1) and type II BICs (II_2, II_3) are located on the interface state (black curve) with the common PBG of PhC1 and PhC2, and the electromagnetic local area is also at the interface of PhC1 and PhC2 of the rotational periodic system. Type III BICs (III_1–III_6) are defined where the bulk bands of PhC1 and PhC2 overlap (red and blue curves), and the electromagnetic locality is also in PhC1 or PhC2 in the rotational periodic system. In other words, type I BICs (BCR modes), type II BICs (BCR modes), and type III BICs are located in PhC1 of the rotational periodic system, the interface between PhC1 and PhC2, and the single circle of PhC1 or PhC2, respectively. Type I BICs (BCR modes), type II BICs (BCR modes) and type III BICs can be used in fiber, while type I and type III BICs (BCR modes) are located in the bulk bands — type II is formed by the interface state extension decoupling. Because these three types of BIC can exist in a model at the same time, the fiber made with such a rotational period structure will expand the BIC frequency band range.

These BCRs are similar to the whispering gallery mode (WGM),[45] and correspond to the WGM in the far-field with the same maximum strength, which can be verified by combining $k_{||}$ and the OAM formula (see Section B of the supplementary material). The result also proves the accuracy of the OAM we calculated in the rotational periodic system.

In conjunction with Figs. 2(a) and 2(b), interface state-based BIC (II_3) and interface state-based BICs in the long-strip supercell (red diamond) coincide (see Section A of the supplementary material). Type II BIC (II_1) and BCR (II_2) are C_{3v} symmetry; we can determine whether they are C_{3v} symmetry-protected by breaking the rotational symmetry.

For type III BICs ($k_{||} \neq 0$), the location of the projected bands in Fig. 2(a) can be calculated using the corresponding OAM formula of the circle. According to the OAM formula, $\beta = k_m R$ (k_m is the azimuth Bloch wave number of the circular

array, R is the radius of the ring where BIC existed),[6,33,45] the OAM of symmetry-protected type III BICs (BCR modes) $\beta^* \approx \beta = MN/2$ (see Section B of the supplementary material).

In order to describe the three types of BICs further and qualitatively in rotational periodic systems, the Neumann boundary conditions[43,44] of rigid cylindrical surfaces and the Graf formula[43] can be introduced for analysis. We briefly enumerate the correspondence between incident amplitude a_m^+ and emanating amplitude $a_{m'}^-$ of type I–type III BICs (BCR modes).

Similarly, we use the subscripts e, p, l, g and u to describe the concentric N (0,1,2,3,4). For type I BICs, the relationship between the incident amplitude and the emanating amplitude of the $(p+1)$-th scatterer surface can be expressed as follows:

$$a_m^+(p+1) = \sum_{e=0}^{M(N-2)} \sum_{p=1}^{M(N-1)} \sum_{l=0}^{MN} \sum_{m'} a_{m'}^- O_{m'}^- H_{m'-m}^{(1)} \times [k_0(r_{e(p+1)} + r_{p(p+1)} + r_{(l+1)(p+1)})], \quad (4)$$

where $a_{m'}^- = a_{m'}^-(e) + a_{m'}^-(p) + a_{m'}^-(l)$, and $O_{m'}^- = \exp[\mathrm{i}m\theta_{p+1} - \mathrm{i}(m-m')(\theta_{e(p+1)} + \theta_{p(p+1)} + \theta_{(l+1)(p+1)}) - \mathrm{i}m'(\alpha_e + \alpha_p + \alpha_{l+1})]$. The details are shown in Section C of the supplementary material.

For type II BICs, the radiation state becomes entirely confined within the interface,

$$a_{m'}^+(l+1) = \sum_{g=1}^{MN} \sum_{l=0}^{M(N-1)} \sum_{u=0}^{M(N+1)} \sum_{m'} a_{m'}^- O_{m'}^- H_{m'-m}^{(1)} \times [k_0(r_{p(l+1)} + r_{l(l+1)} + r_{g(l+1)})], \quad (5)$$

where $a_{m'}^- = a_{m'}^-(l) + a_{m'}^-(p) + a_{m'}^-(g)$, and $O_{m'}^- = \exp[\mathrm{i}m\theta_{l+1} - \mathrm{i}(m-m')(\theta_{l(l+1)} + \theta_{g(l+1)} + \theta_{p(l+1)}) - \mathrm{i}m'(\alpha_p + \alpha_g + \alpha_l)]$.

Type III BICs are mainly affected by the adjacent scatterers in the ring,

$$a_m^+(g+1) = \sum_{g=1}^{MN} \sum_{l=0}^{M(N-1)} \sum_{u=0}^{M(N+1)} \sum_{m'} a_{m'}^- O_{m'}^- H_{m'-m}^{(1)} \times [k_0(r_{g(g+1)} + r_{(l+1)(g+1)} + r_{(u+1)(g+1)})], \quad (6)$$

where $a_{m'}^- = a_{m'}^-(g) + a_{m'}^-(l+1) + a_{m'}^-(u+1)$, and $O_{m'-} = \exp[\mathrm{i}m\theta_g - \mathrm{i}(m-m')(\theta_{g(g+1)} + \theta_{(l+1)(g+1)} + \theta_{(u+1)(g+1)}) - \mathrm{i}m'(\alpha_g + \alpha_{l+1} + \alpha_{u+1})]$.

For ease of calculation, only the influence of the two nearest neighbor rings is considered. Based on the scattering theory of the C_{6v} rotational periodic system, the formulas for calculating three types of BICs (BCR modes) are derived, and a general theory is proposed that can be extended to the C_{nv} rotational periodic system, which indicates that the dispersion equation of BICs and BCR modes can be solved by utilizing eigenvectors when the value of M and N conforms to the formula $\sum_m a_{m'n}^- J_{n-m}(k_0 R_g) = 0$ (see Section C of the supplementary material).

In order to verify the universality of the theory of three types of BICs and BCR modes in the rotational periodic system, we also design rotational periodic systems with different parameters to verify the theory (see Section D of the supplementary material).

To refine the classification of BICs (BCR modes), we changed the rotational periodic system from C_{6v} to C_{5v} symmetries, thereby breaking the C_{3v} symmetry while keeping the other parameters constant. The results are shown in Fig. 3.

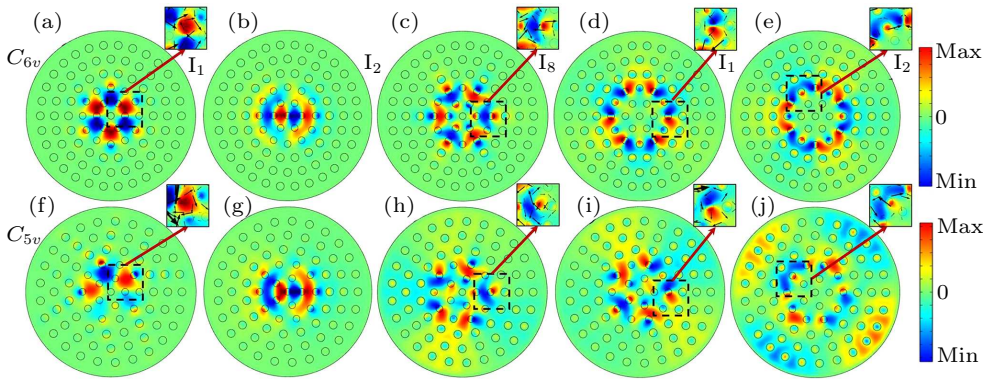


Fig. 3. Off-Γ: type I BCR modes (I_1, I_2), type I BICs (I_8); Off-Γ type II BCR mode (II_1), type II BIC (II_2); (a)–(e) C_{6v}; (f)–(j) C_{5v}.

As shown from Fig. 3(a) to Fig. 3(e), it can be observed that, with the exception of the E_z field of non-electromagnetic dissipations, the Poynting vector arrows corresponding to the E_z fields of the C_{6v} and C_{5v} symmetries are in the same direction of rotation and topological winding at high symmetry.

It proves that the graph below is the resonance of the graph above which reduces the symmetry. The severe electromagnetic dissipation that occurs after the reduction of symmetry is shown in Figs. 3(a)–3(e) except Fig. 3(b). Therefore, Figs. 3(b) and 3(g) are non-symmetry-protected BCR modes, and the rest are symmetry-protected BICs (BCR modes).

Since the rotational symmetry of the system has little effect on the non-symmetry-protected BICs (BCR modes), we will focus on the relationship between the Q factors of the

symmetry-protected BICs (BCR modes) and rotational symmetry. We have calculated the Q factors of three types of BICs (BCR modes) in Fig. 4.

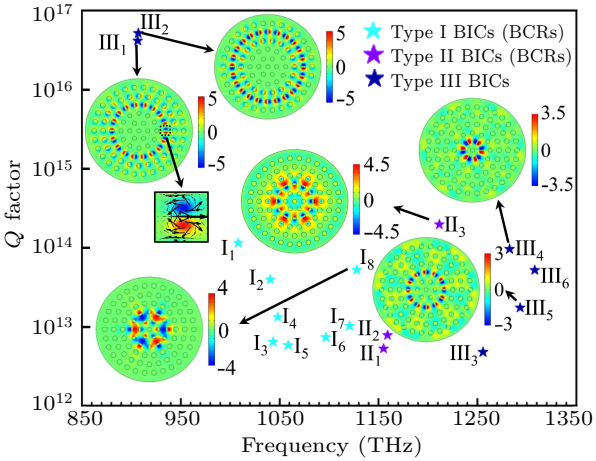


Fig. 4. The Q factors of three types of BICs and BCR modes, and part of the E_z field.

It shows that type I BIC (I_8), type I BIC (II_3) and type III BIC (III_2) with the highest Q factor are all protected by higher symmetry than other BICs in these types, as well as in the BCR modes.

In other words, the resonance with the highest symmetry possesses the highest Q factor. The Q factors of the BCR modes and BICs are similar in order of magnitude. This is due to the cancelation of multiple scattering between scatters; the different radiation channels of the three BCRs destructively interfere with each other in the far-field, which makes the Q factor of the BCR modes higher and proves that BCR modes in the rotational periodic system have more potential.

In addition to the III_5, for the rest of the type III BICs (III_1, III_2, III_4), the Q factor associated with N in which BICs is located. In order to explore the relationship between the Q factor and the concrete structure (M and N) of symmetry-protected BICs, we chose symmetry-protected type III BICs to explore the influence of different M and N on the Q factor. According to the calculation of the real and imaginary parts of type III BICs, the Q factor is proportional to MN, which indicates it remains unchanged after the exchange of values of M and N under certain conditions (see Section E of the supplementary material). III_5 is because its circle is located near the interface, and different scatterers in the adjacent circle cause radiation states which cannot be completely canceled, resulting in a smaller Q factor than that of III_4.

Such a rotational periodic system with multi significantly reduces large bending losses and increases Q factors of BIC and BCR modes.[26,32,33] The generation of BIC has certain requirements for the precision of the structural design, and small errors in the machining process may cause the deviation of BICs and the expected experimental results.[28] The model designed by us improves its robustness by increasing the Q factors of BICs and BCR modes, and reduces the errors caused in the manufacture of experimental models. Moreover, off-Γ BICs designed by us are less prone to damage than the symmetry-protected BICs at Γ points,[47,48] which enhances the feasibility of the experiment.

4. Conclusion

In conclusion, we have developed a novel method for identifying three types of BICs and BCR modes (type I–type III) based on electromagnetic characterization and band positions. These BICs and BCR modes based on the bulk bands of two PhCs serve to expand the frequency range and offer possibilities for designing photonic devices based on near-BICs (BCR modes) of the rotational periodic system. We calculate the OAM of the rotational periodic system by transforming the Bloch wave number from the translational periodic system, thus providing a general theory about BICs and BCR modes of the rotational period system of C_{nv}. Our results demonstrate that these BICs and BCR modes exhibit a low material loss rate and possess high-Q factors, surpassing most of the quasi-BICs and BCR modes presently available, expanding the research potential and application area of BCR modes in photonic devices. Additionally, we have identified that increasing the values of M and N can increase the Q factor of symmetry-protected BICs.

Acknowledgements

This work was supported by the National Natural Science Foundation of China (Grant Nos. 61405058 and 62075059), the Natural Science Foundation of Hunan Province (Grant Nos. 2017JJ2048 and 2020JJ4161), and the Scientific Research Foundation of Hunan Provincial Education Department (Grant No. 21A0013), the Open Project of State Key Laboratory of Advanced Optical Communication Systems and Networks of China (Grant No. 2024GZKF20), and the Guangdong Basic and Applied Basic Research Foundation (Grant No. 2024A1515011353).

References

[1] Schult R L, Ravenhall D G and Wyld H W 1989 *Phys. Rev. B* **39** 5476
[2] Hsu C W, Zhen B, Chua S L, Johnson S G, Joannopoulos J D and Soljačić M 2013 *Light Sci. Appl.* **2** e84
[3] Zhang Y W, Chen A, Liu W Z, Hsu C W, Wang B, Guan F, Liu X H, Shi L, Lu L and Zi J 2018 *Phys. Rev. Lett.* **120** 186103
[4] Robnik M 1986 *J. Phys. A: Math. Gen.* **19** 3845
[5] Bulgakov E N and Sadreev A F 2014 *Phys. Rev. A* **90** 053801
[6] Bulgakov E N and Sadreev A F 2017 *Phys. Rev. A* **96** 013841
[7] Sadrieva Z F, Belyakov M A, Balezin M A, Kapitanova P V, Nenasheva E A, Sadreev A F and Bogdanov A A 2019 *Phys. Rev. A* **99** 053804
[8] Lu C C, Wang C Y, Xiao M, Zhang Z Q and Chan C T 2021 *Phys. Rev. Lett.* **126** 113902

[9] Shi A Q, Peng Y W, Jiang J P, Peng Y C, Peng P, Chen J Z, Chen H S, Wen S C, Lin X, Gao F and Liu J J 2024 *Laser Photonics Rev.* **18** 2300956
[10] Yan B, Peng Y W, Xie J L, Peng Y C, Shi A Q, Li H, Gao F, Peng P, Jiang J P, Liu J J, Gao F and Wen S C 2024 *Laser Photonics Rev.* **18** 2470035
[11] Yang Y, Peng C, Liang Y, Li Z B and Noda S 2014 *Phys. Rev. Lett.* **113** 37401
[12] Bulgakov E N and Sadreev A F 2016 *Phys. Rev. A* **94** 033856
[13] Hu Z and Lu Y Y 2018 *J. Phys. B* **51** 035402
[14] Zhen B, Hsu C W, Lu L, Stone A D and Soljačić M 2014 *Phys. Rev. Lett.* **113** 257401
[15] Doeleman H M, Monticone F, Hollander W D, Alù A and Koenderink A F 2018 *Nat. Photonics* **12** 397
[16] Neumann J V and Wigner E P 1929 *Phys. Z.* **30** 465
[17] Ursell F 1987 *J. Fluid Mech.* **183** 421
[18] Evans D V and Linton C M 2006 *J. Fluid Mech.* **225** 153
[19] Jiang X W, Fang B and Zhan C L 2024 *Chin. Phys. B* **33** 034206
[20] Wu F, Wu J J, Guo Z W, Jiang H T, Sun Y, Ren J and Chen H 2019 *Phys. Rev. Appl.* **12** 014028
[21] Zeng J and Li Z Y 2022 *Chin. Phys. B* **31** 043202
[22] Wang J J, Shi L and Zi J 2022 *Phys. Rev. Lett.* **129** 236101
[23] Wu F, Liu T T, Long Y, Xiao S Y and Chen G Y 2023 *Phys. Rev. B* **107** 165428
[24] Evans D V, Levitin M and Vassiliev D 1994 *J. Fluid Mech.* **261** 21
[25] Longhi S 2006 *Eur. Phys. J. B* **57** 45
[26] Bulgakov E N and Sadreev A F 2018 *Phys. Rev. B* **98** 085301
[27] Plotnik Y, Peleg O, Dreisow F, Heinrich M, Nolte S, Szameit A and Segev M 2011 *Phys. Rev. Lett.* **107** 183901
[28] Cerjan A, Hsu C W and Rechtsman M C 2019 *Phys. Rev. Lett.* **123** 023902
[29] Ardizzone V, Riminucci F, Zanotti S, Gianfrate A, Efthymiou-Tsironi M, Suàrez-Forero D G, Todisco F, De Giorgi M, Trypogeorgos D, Gigli G, Baldwin K, Pfeiffer L, Ballarini D, Nguyen H S, Gerace D and Sanvitto D 2022 *Nature* **605** 447
[30] Chen Y, Deng H, Sha X, Chen W J, Wang R, Chen Y H, Wu D, Chu J, Kivshar Y S, Xiao S and Qiu C W 2023 *Nature* **613** 474
[31] Xiao S S and Qiu M 2005 *Phys. Lett. A* **340** 474
[32] Han H L, Lü H B and Liu X 2018 *Opt. Lett.* **43** 5403
[33] Bulgakov E N and Sadreev A F 2018 *Phys. Rev. A* **97** 033834
[34] Molina M I, Miroshnichenko A E and Kivshar Y S 2012 *Phys. Rev. Lett.* **108** 070401
[35] Corrielli G, Della Valle G, Crespi A, Osellame R and Longhi S 2013 *Phys. Rev. Lett.* **111** 220403
[36] Longhi S and Della Valle G 2013 *J. Phys. C: Cond. Mat.* **25** 235601
[37] Chai J W, Liu L, Hu P, Xiang H and Han D Z 2020 *Opt. Lett.* **45** 5652
[38] Wang W H, Srivastava Y K, Tan T C W, Wang Z and Singh R 2023 *Nat. Commun.* **14** 2811
[39] Wu L H and Hu X 2015 *Phys. Rev. Lett.* **114** 223901
[40] Yoda T and Notomi M 2020 *Phys. Rev. Lett.* **125** 053902
[41] Huang X Q, Xiao M, Zhang Z Q and Chan C T 2014 *Phys. Rev. B* **90** 075423
[42] Horvath H 2009 *J. Quant. Spectrosc. Radiat. Transfer* **110** 787
[43] Maystre D, Enoch S and Tayeb G 2006 *Electromagnetic Theory and Applications for PhC* (USA:CRC) p. 46
[44] Linton C M and Evans D V 1990 *J. Fluid Mech.* **215** 549
[45] Burin A L, Blaustein G S and Samoylova O M 2006 *Phys. Rev. E* **73** 066614
[46] Oraevsky A N 2002 *Quantum Electr.* **32** 377
[47] Ni L F, Wang Z X, Peng C and Li Z B 2016 *Phys. Rev. B* **94** 245148
[48] Yuan L J and Lu Y Y 2020 *Phys. Rev. A* **101** 043827